International Journal of Coal Geology 165 (2016) 76–89

Contents lists available at ScienceDirect

International Journal of Coal Geology

journal homepage: www.elsevier.com/locate/ijcoalgeo

Microstructures of Early Jurassic (Toarcian) shales of Northern Europe

M.E. Houben [a,*], A. Barnhoorn [b], L. Wasch [c], J. Trabucho-Alexandre [a], C.J. Peach [a], M.R. Drury [a]

[a] Faculty of Geosciences, Utrecht University, PO-box 80.021, 3508TA Utrecht, The Netherlands
[b] Faculty of Civil Engineering & Geosciences, Delft University of Technology, PO-box 5048, 2600GA Delft, The Netherlands
[c] TNO, Princetonlaan 6, 3584 CB Utrecht, The Netherlands

ARTICLE INFO

Article history:
Received 7 January 2016
Received in revised form 4 August 2016
Accepted 4 August 2016
Available online 06 August 2016

Keywords:
Posidonia Shale
Whitby Mudstone
Clay microstructure
Ion-beam polishing
Scanning Electron Microscopy
X-ray diffraction

ABSTRACT

The Toarcian (Early Jurassic) Posidonia Shale Formation is a possible unconventional gas source in Northern Europe and occurs within the Cleveland Basin (United Kingdom), the Anglo-Paris Basin (France), the Lower Saxony Basin and the Southwest Germany Basin (Germany), and the Roer Valley Graben, the West Netherlands Basin, Broad Fourteens Basin, the Central Netherlands Basin and the Dutch Central Graben in The Netherlands. Outcrops can be found in the United Kingdom and Germany. Since the Posidonia Shale Formation does not outcrop in the Netherlands, sample material suitable for experimental studies is not easily available. Here we have investigated lateral equivalent shale samples from six different locations across Northern Europe (Germany, The Netherlands, The North sea and United Kingdom) to compare the microstructure and composition of Toarcian shales. The objective is to determine how homogeneous or heterogeneous the shale deposits are across the basins, using a combination of Ion Beam polishing, Scanning Electron Microscopy and X-ray diffraction. The work presented here shows that the Toarcian shales of Northern Europe display considerable homogeneity in mineralogy and microstructure in the different investigated samples and formations, where the largest variability is the carbonate content ranging from almost zero up to 80%. We conclude that the outcrop locations in Germany and the United Kingdom are suitable analogues with respect to their mineralogy and microstructure for experimental studies on the Posidonia Shale in the Dutch subsurface.

1. Introduction

The Toarcian (Early Jurassic) Posidonia Shale Formation (PSF) is one of the main hydrocarbon source rocks in the North Sea (Germany and The Netherlands) as well as in the Paris Basin (Tissot and Welte, 1978) with a thickness of circa 10 up to 70 m (30 m on average) and an average total organic carbon (TOC) content of 10% (Herber and de Jager, 2010). The lower Toarcian shales were deposited in the Cleveland Basin (Whitby Mudstone Formation), the Lower Saxony Basin, the Southwest Germany Basin (Posidonia Shale Formation) and the Anglo-Paris basin ('Schistes Carton'; e.g. Rullköter et al., 1988; Littke et al., 1991; Fig. 1). Lower Jurassic shales in the North Sea Basin are generally dark grey, thin bedded and bituminous, and they were deposited in an epicontinental shelf sea with variable energetic conditions and periodic benthic oxygen depletion (e.g.: Trabucho-Alexandre et al., 2012; French et al., 2014). The PSF in the Hils Area in Germany represents a large maturity range, from very early mature to over mature gas window (Littke et al., 1991). The formation only reaches gas maturity in small isolated synclines in the deepest parts of the West Netherlands Basin and Roer Valley Graben (de Jager et al., 1996). The lower and upper boundaries of PSF are geochemically and petrographically abruptly bounded by less organic matter rich and less carbonate rich shales at the bottom and top that are displaying a lower hydrogen index than the Posidonia Shale Formation (Littke et al., 1991). Posidonia Shale units are fine-grained with porosities below 10 vol.% (Littke et al., 1991). On mechanically polished thin sections, no obvious visible primary connected pathways that might act as permeable conduits for the expulsion of fluids or gasses, are present in the PSF (Littke et al., 1988).

Interest in the PSF has increased since it was recognised as a possible source for unconventional oil/gas in Northern Europe (e.g.: Herber and de Jager, 2010). The work presented here summarizes the microstructures encountered in PSF samples sampled from cores and outcrops from the current North Sea basin and surrounding countries (Germany, The Netherlands and United Kingdom) with the aim to investigate how microstructurally and mineralogically similar the deposits are throughout the sampled areas. Our aim is to determine the variability of Toarcian shales in the North Sea Basin and surrounding countries and to validate the use of outcrop samples for experimental studies as mechanical and petrophysical characterization, permeability and swelling/shrinking experiments. Characterization of the samples is a first step to better understanding ways to enhance the permeability of the rock and to increase gas flow from the rock to well.

* Corresponding author.
E-mail address: m.e.houben@uu.nl (M.E. Houben).

http://dx.doi.org/10.1016/j.coal.2016.08.003

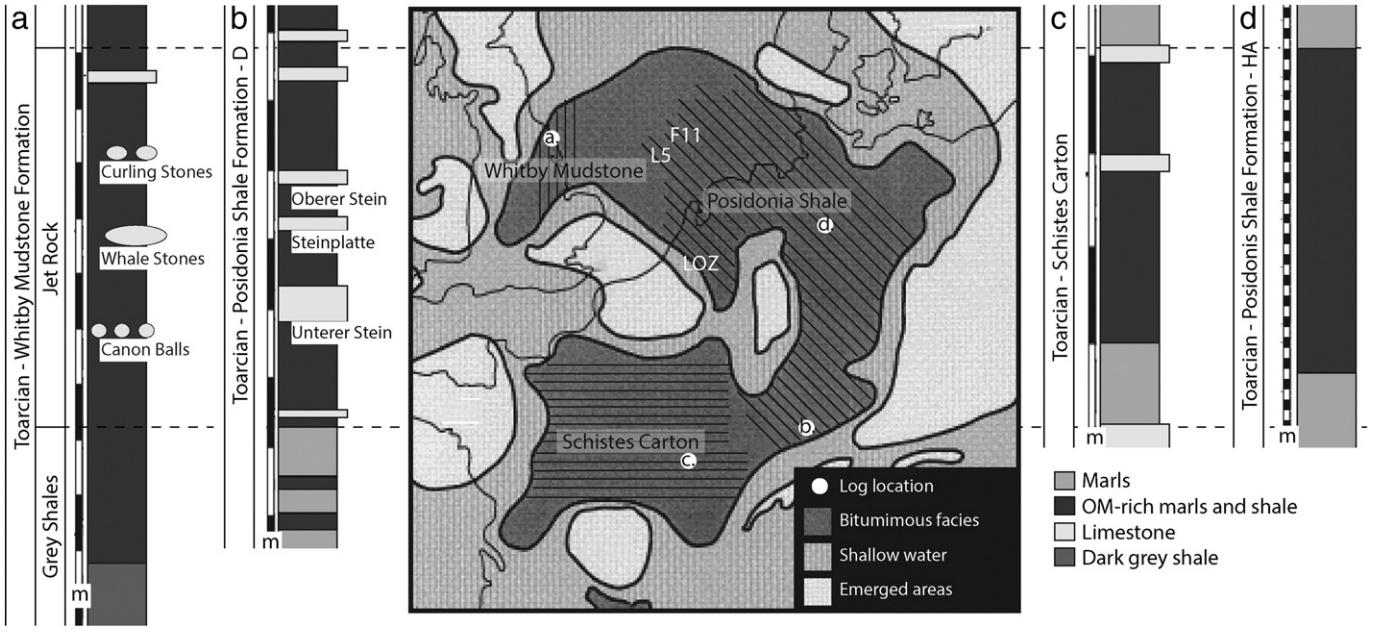

Fig. 1. Sedimentary logs of the Toarcian deposits of organic matter rich marls and shales deposited in the current North Sea basin and a map of the North Sea basin during the Sinemurian Aalenian modified after Röhl et al. (2001). Sample locations are indicated in the map either by the letters a.–d. corresponding to the logs or by the abbreviations used in the paper (F11, L5 and LOZ). a. Jet rock section of the Whitby Mudstone modified after Hesselbo et al., 2000. b. Posidonia Shale from Dotternhausen (DE) modified after Röhl et al., 2001. c. Schistes Carton from the Paris Basin modified after Emmanuel et al., 2006. d. Posidonia Shale from the Hils Area (DE) modified after Littke et al., 1991.

2. Materials

2.1. Posidonia Shale Formation and Whitby Mudstone Formation samples

We investigated two samples from the Loon-op-Zand core (sample numbers S37 and S41; PSF-LOZ) which was cored in the West Netherlands Basin (the Netherlands) in the 1950s. The two samples originate from the lower half of the PSF section. Sample S37 was cored at a depth of circa 2495 m and sample S41 originated from a depth of circa 2507 m. Other PSF samples investigated, originated from the North Sea Basin (L5-4 core; PSF-L5) and were cored in 1985. The PSF interval was cored at a depth of 2824.65 to 2842.40 m. Four 1.2 cm diameter drill-cores and nine thin sections were used for microstructural research. Furthermore, nine PSF thin sections from well F11-01 (North Sea Basin, Dutch Central Graben; PSF-F11) were investigated, where the samples originated from depths between 2657 and 2672 m. PSF samples were also collected at a quarry in Dotternhausen (Germany) in 2009 (PSF-D). The sample block used for microstructural research was taken in the quarry. The Whitby Mudstone Formation (WMF) samples were sampled along the cliff coast north of Whitby in the United Kingdom near Runswick Bay and Port Mulgrave (see also Zhubayev et al., 2016). Location of the different samples can be found in Fig. 1. All samples were stored under atmospheric conditions and hence were air-dried during sample storage, either up to 60 years for some of the PSF samples or a couple of months for the WMF samples.

3. Methods

3.1. Scanning Electron Microscopy

Both mechanical polished thin sections (circa 2.5 × 4 cm) produced using conventional methods and argon ion beam polished samples using a Precision Ion Polishing System (PIPS; 8 mm in diameter; Houben et al., 2016) were investigated with Scanning Electron Microscopes (SEM: FEI XL30S FEG-SEM; FEI Nova 600 Nanolab; JEOL Neoscope II JCM-6000). All samples were polished perpendicular to the bedding. Identification of pores and small minerals requires both good spatial and contrast resolution, which depends on the quality of the final sample polish, the SEM instrument, its detector capabilities and the imaging conditions used. The mechanically polished thin sections displayed good enough spatial resolution (300 nm pixel size, meaning minerals >1 μm in diameter could be imaged) to get information about the mineralogy and the microstructure of the sample. PIPS polished SEM samples were used to investigate both the mineralogy and the porosity (circa 25 nm pixel size, meaning only pores with diameters >100 nm were imaged). With a Back Scattered Electron (BSE) detector density contrast in the micrographs was displayed to investigate the mineralogical variation in the samples in combination with an Energy-dispersive X-ray (EDX) detector. The grey scales in a BSE image from black to white correspond to: pores/cracks, organic matter, matrix/clay minerals/quartz/feldspar, calcite/dolomite, pyrite (see also Klaver et al., 2015a; Houben et al., 2016). In addition, the SEM's Secondary Electron (SE) detector has been used to image the pores in the PIPS-SEM samples. In order to make high resolution images of the PIPS-SEM samples in combination with imaging a large area, single SEM images were combined into one high resolution mosaic image using Microsoft Image Composite Editor. For the PIPS-SEM samples a low magnification (200×) was used to make an overview image of the whole PIPS polished cross-section. Subsequently high resolution mosaics (magnification 5.000×) were made, aimed at mineralogically different layers, to image the 2D sample microstructures using the BSE detector. The high resolution BSE and SE mosaics were made in regions in between the largest cracks. The microstructures present in the mechanically polished thin sections were imaged with a slightly different approach; a single BSE image covering circa 300 × 400 μm^2 was made (pixel size 300 nm). The image was made in an area without any large cracks running through the entire polished section. In combination with EDX maps for the elements Si, Al, Ca, Mg, Fe, Na, K, and S the mineralogy in that single image was identified. Visible minerals (grains with diameters >2 μm; silicates (quartz, feldspar), carbonates (calcite, dolomite), pyrite, organic matter) in both the thin sections and PIPS-SEM samples were segmented, either by using a combination of thresholding and edge detection in MATLAB 2010 (for pyrite and organic matter only) or manually using ArcMAP 10.1 (silicates, carbonates, mica's and clay minerals) by making use of the BSE images and EDX maps.

3.2. X-ray diffraction

$Q_{mineral}$ Analysis & Consulting (Heverlee, Belgium) identified and quantified both the bulk mineral composition and the mineralogy of the clay fraction. Samples were oven dried (40 °C) and ground before X-ray diffraction using CuK_{α} radiation (Środoń et al., 2001). During the first stage of the experiment bulk mineralogy was investigated with Rietveld analysis (Rietveld, 1967) using the TOPAS software from Bruker. During the second stage of the experiment 5 g of the initial sample material was selectively disintegrated from aggregates that incorporate clay minerals (Jackson treatment; Jackson et al., 1976) and the fraction of the sample smaller than 2 μm was dissociated from the bulk by centrifugation. Oriented clay samples were prepared and used for the XRD analysis where quantification was done using the PONKCS-methods in the NEWMOD2 software (Moore and Reynolds, 1997; Scarlett and Madsen, 2006).

4. Results

4.1. SEM

A selection of microstructures encountered in the investigated samples can be found in Figs. 2 and 3. Comparing the sample overviews (Fig. 2) shows that some samples are more fractured than others. Whether these fractures are due to drilling, drying, sample preparation, or a combination of all is not clear, but the fractures are interpreted as not being part of the in-situ microstructure (see also Houben et al., 2013). Smaller cracks with widths up to about 1 μm account for up to 20% of the visible porosity in the PIPS-SEM mosaics, where some samples are more affected than others. Microcrack shape, length and amount seems to be related to the microstructure/cementation of the sample and not to storage or drying time since no trend is visible that longer storage and hence longer drying or origination from lower depths generates more cracks in the microstructure of the different samples. Most cracks run through the matrix and surround the larger minerals. In addition, some sample overviews display mineralogically diverse layers easily differentiated based on the overall grey colour present in that certain layer in the overview (e.g. Fig. 2b) and the different microstructures in the high resolution mosaics (Fig. 3). Most samples show a dark grey fine grained matrix wherein organic matter (black) and pyrite (white) are easily distinguished from the background and single quartz, mica, calcite and dolomite grains are also present mostly floating within the matrix (Fig. 3). Organic matter is usually distributed along the bedding, present in very elongated patches and is mostly non-porous in all investigated samples. Pyrite is mainly present as framboidal pyrite up to circa 10 μm in diameter, where the individual pyrite grains present are up to 5 μm in diameter. The largest fossils present show diameters up to 1 mm (Fig. 2c).

All high resolution mosaics covered an area >300 × 300 μm^2. The areas were large enough to be called representative for the specific imaged layer considering organic matter, silicate and carbonate minerals, pyrite, matrix (all minerals/grains with a diameter <2 μm) and fossils (when present) as main phases using the point counting method (e.g.: Kameda et al., 2006). After the image exceeds 150 × 150 μm^2 the mineralogy within the images stabilized and if the imaged area exceeds 200 × 200 μm^2 the mineral content does not vary >2% on average anymore when box sizes were increased, implying that 200 × 200 μm^2 can be interpreted as the representative elementary area for microstructure (REA; Fig. 4). Fig. 4 furthermore gives an impression of the heterogeneity present within one formation, but mainly visible in the graphs are the differences and similarities between the samples originating from different locations within the basin. For example, about half of the PSF-L5 samples show lower amounts of matrix and higher amounts of silt-sized minerals (larger than 2 μm) present in the mosaics (Fig. 4). Furthermore the WMF, PSF-L5 and PSF-F11 samples display on average a slightly lower organic matter content than found in the PSF-LOZ and PSF-D samples. PIPS-SEM high resolution mosaic mineralogy and SEM thin section mineralogy is summarized in Table 1 also illustrating the mineralogical differences and similarities found in the different layers within one PIPS-SEM sample. Indicated in the tables heading are relative variabilities per mineral phase, these are averaged over the whole dataset to get an idea of the variation in that mineral phase from an area of circa 150 μm × 150 μm onwards and can be used as the error bar for SEM mineralogy measurements (Table 1). The pyrite content in all investigated samples varies between 1 and 7 area% and the framboidal pyrite is homogeneously spread throughout the images. The organic matter content varies per sample from 3.4–37.4 area% (Table 1). Where the WMF samples show an organic matter content in the range of 3.4 to 8.1 area%, the PSF-D shows an organic matter content of 16.3 area%, the two PSF-LOZ samples show average organic matter contents of 23.5 area% (PSF-LOZ-37) and 10.3 area% (PSF-LOZ-41), the PSF-L5 samples show on average organic matter content of 14.0 area% and the PSF-F11 samples display an average organic matter content of 9.5 area% (Table 1). Matrix amounts (clay minerals and all mineral grains with a diameter below 2 μm) vary per sample and per section; WMF 59.1–76.8 area%, PSF-LOZ 50.6–74.5 area%, PSF-D 55.3–56.3 area%, PSF-L5 30.1–85.0 area%, PSF-F11 24.8–88.6 area% (Table 1). Most samples show matrix contents >50 area%, the low values for one of the PSF-F11 and some of the PSF-L5 samples are due to the high amounts of large (>50 μm in diameter) carbonate minerals (dolomite) in these samples. Carbonate values range from circa 0 up to 60 area% (Table 1). The samples can be microstructurally subdivided into samples with porous calcite fossils (the porous fossils are surrounded in the high resolution mosaics with white lines; Fig. 3) and samples without. Fossil rich samples were mainly found in samples originating from the top half of the section that were deposited at the basins edge (WMF, PSF-LOZ,

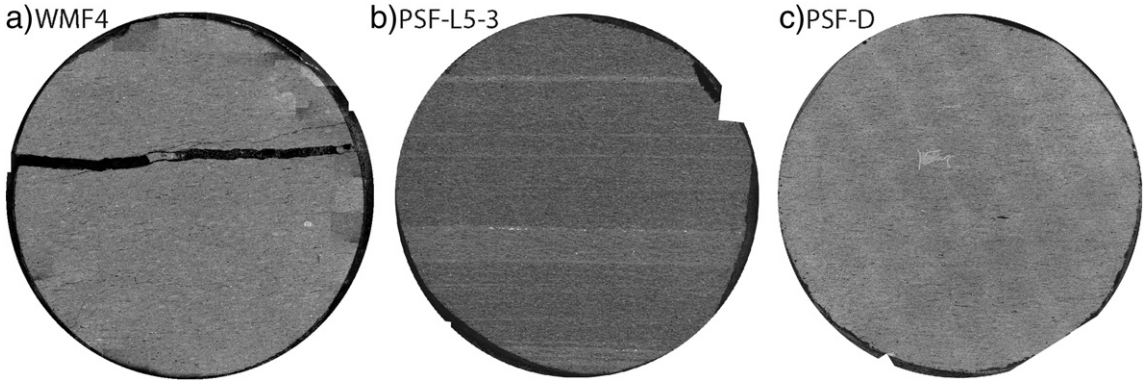

Fig. 2. Three PIPS polished SEM samples with sample diameters of 8 mm. a. WMF 4 with a large crack running through the sample along the bedding. b. PSF-L5-3 a mineralogically layered sampled on the sub-mm scale. c. PSF-D typical intact sample with larger fossil fragments visible in the sample overview.

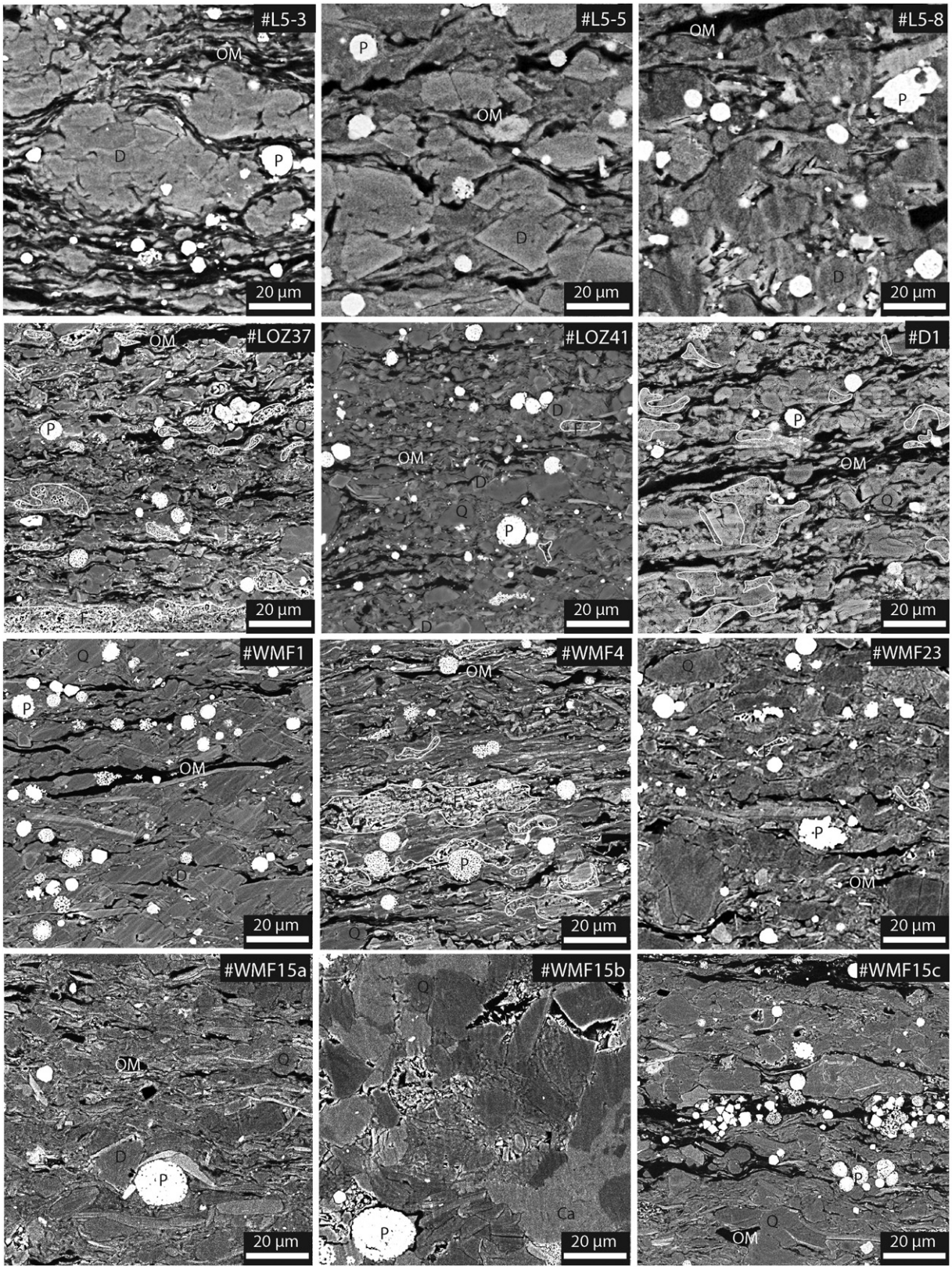

Fig. 3. A selection of the microstructures encountered in the PSF and WMF samples from different locations. As a comparison for WMF15 (bottom row) high resolution mosaics made within one PIPS-SEM sample are displayed illustrating the difference in microstructure not only encountered in samples from different locations but also from within one sample. Sample locations within the basin can be found in Fig. 1.

PSF-D). PSF-L5 and PSF-F11 samples, derived from the middle of the North Sea, show layers with high carbonate contents as well, but in this case that is due to large (up to 60 μm in diameter) dolomite grains interlayered with organic matter and matrix. These dolomite rich (carbonate) layers are again mainly present in the upper half of the section in the F11 and L5 cores. PSF-LOZ-41 does show a relatively high amount

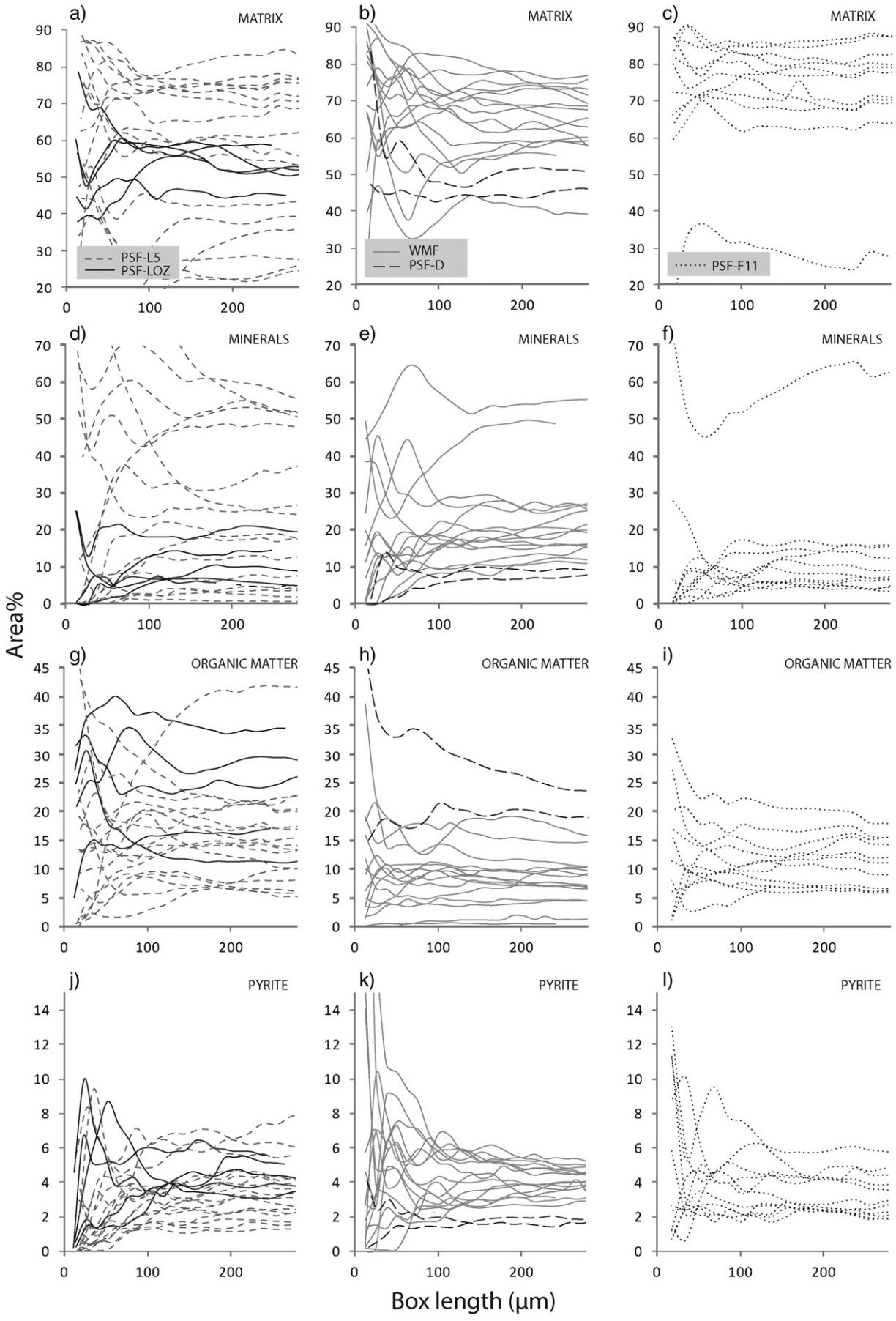
a)
MATRIX
PSF-L5
PSF-LOZ
b)
MATRIX
WMF
PSF-D
c)
MATRIX
PSF-F11
d)
MINERALS
e)
MINERALS
f)
MINERALS
g)
ORGANIC MATTER
h)
ORGANIC MATTER
i)
ORGANIC MATTER
j)
PYRITE
k)
PYRITE
l)
PYRITE
Area%
Box length (µm)

of dolomite as well (2–10%), but the dolomite grains have diameters smaller than 10 μm in the PSF-LOZ-41 sample and do not dominate the microstructure as in the PSF-L5 and PSF-F11 samples (Fig. 3). Visible porosity present in the SEM images is mainly situated in the matrix (Fig. 5a, b; interparticle pores; Desbois et al., 2009), and within the calcite fossils (e.g. coccolithophores, *Schizosphaerella*; Fig. 5d-f), which are intraparticle pores (Loucks et al., 2012). Carbonate fossils with pores as in Fig. 5f are most abundant and porosity values within these fossils are ranging up to 11 area%. Furthermore, porosity is found in all samples in between loosely packed pyrite grains forming framboidal pyrite (interparticle pores; Fig. 5g). In addition, porosity is present in some of the organic matter (intraparticle pores; Fig. 5h), in mica (Intraparticle pores; Fig. 5i), and around mineral grains dissolution pores or pores interpreted due to drilling and stress relaxation are present (interparticle pores; Fig. 5 j-m). Visible porosity depends on the image resolution and although resolution is similar for all mosaics the values vary per mosaic and are in the order of 0.3–2.5 area% (Table 1; see also Houben et al., 2016).

4.2. X-ray diffraction

The XRD bulk measurements show that the PSF-LOZ samples are more carbonate rich than the WMF samples (Table 2). In addition the total amount of sheet silicates (illite, illite/smectite, kaolinite, chlorite) is lower in the LOZ core than the amounts found in the WMF samples. The amount of sheet silicates is inversely related to the carbonate content. Furthermore, the results show that the silicate contents (mainly quartz) are constant throughout the WMF and LOZ sections. Values vary between 12.8 and 18.3 wt% with one exception in the LOZ core (silicate content of 30.5 wt%). Pyrite contents in the WMF and LOZ cores overlap, but the values for the WMF samples are on the high end (7.7–11 wt%) when compared to the LOZ results (3.8–9.4 wt%). The clay fraction XRD data does not show big differences between the two cores. Interlayered illite/smectite, illite and kaolinite are approximately evenly distributed in the clay fraction with some minor amounts of chlorite (1–4 wt%).

5. Discussion

5.1. Representative Elementary Area

Using the box counting method to investigate Representative Elementary Area (REA) for mineral fraction resulted in a REA of 200 μm × 200 μm (when using a mineralogy fluctuation of <2% from one box to the next). The overall mineral fraction within a box of changing dimension was taken into account in the REA analyses, not the grain sizes of the different minerals. The larger scale mineral fabric was only taken into account in a qualitative way. Mosaics were made in such a way that the imaged area contained only one particular mineral fabric. When the mineralogy and thus mineral fabric changed visibly (e.g. Fig. 2b), a separate mosaic was made representative for the other mineral fabric/layer. It is also assumed that the REA for the total visible porosity has the same size as the REA for the mineral fraction (Houben et al., 2013). A REA of 200 μm × 200 μm (Fig. 4) is comparable to the REA as identified for other shales using similar methods (Posidonia Shale Hils Area 140 μm × 140 μm: Klaver et al., 2012; Haynesville and Bossier Shales 200 μm × 200 μm: Klaver et al., 2015a; Opalinus Clay 250 μm × 250 μm: Houben et al., 2014; Boom Clay 155 μm × 155 μm: Hemes et al., 2013, 2015), but only accounts for mineralogy within a certain layer on the (sub-) millimetre scale. It could be that one cm sized sample exists of mineralogically and microstructurally different layers that all could be imaged within 200 μm × 200 μm boxed areas to be representative for the single layers. Cm-sized samples that do show layering on the mm and sub-mm scale should be represented by 3–4 mineralogically different REA's which should be stacked together for upscaling to the centimetre scale (see for example WMF 15; Fig. 3). The thickness of the mineralogically homogenous layers should be known to be able to predict the mineralogy of a centimetre sized sample so that different microstructural homogeneous areas could be accurately stacked together similar to the elementary building block model (Fig. 6; Desbois et al., 2011; Houben et al., 2014). Combining the mineral information from all high resolution mosaics, in their right proportions, then adds up to a SEM mineralogy for WMF 15 of: clay matrix – 69.4 area%, silicates – 11.3 area%, carbonates – 3.1 area%, sulfides – 3.6 area% and organic matter of 7.7 area% (Fig. 6). The SEM mineral content can be compared to the XRD results assuming densities for respectively clay matrix, silicates, carbonates, and sulfides of 2.68, 2.65, 2.71, and 4.9 g/cm^3. For SEM versus XRD data we than find 77 (SEM) versus 69 (XRD) weight% clay matrix, 12 (SEM) versus 17 (XRD) weight% silicates, 3 (SEM) versus 5 (XRD) weight% carbonates, and 7 (SEM) versus 8 (XRD) weight% sulfides. We conclude that carbonate and sulfide contents give really similar results, whereas the silicate content is slightly underestimated and the clay matrix content is overestimated using the SEM method.

5.2. Porosity

Most porous mineral phase in the samples are the carbonate fossils (Fig. 5 d–f) with porosities up to 11%. Although these fossils are highly porous and were encountered in only some samples the total visible porosity of these samples with fossils was not exceeding the visible porosity of the samples without fossils. The occurrence of porous fossils is hence not influencing the total fluid storage or fluid migration capacity. Although these fossils can locally (μm-scale) contribute to higher fluid storage capacities (pockets of fluids) these fossils are not interconnected in 2D, meaning that any flow in and/or out of the rock has to go through the matrix which is the only connected medium visible. This is confirmed by Klaver et al. (2016) who found similar results for Posidonia Shale (Hils Area) in 3D, using a combination of Wood's metal intrusion and SEM imaging. Klaver et al. (2016) show that Wood's metal only intruded little of the samples and intruded mainly areas close to the samples outside meaning that pores in the PSF Hils Area samples are connected with pore throats smaller than 10 nm in diameter which are mostly present in the clay matrix (see also Klaver et al., 2015b).

Furthermore, Mathia et al. (2016) show that the results presented here with respect to distribution of the visible porosity are comparable to the results of the Wickensen and Harderode wells in the Hils Area (Germany) which both plot halfway between inter and intraparticle pores with a maximum of circa 12 area% of organic matter pores (Fig. 5c). The Haddessen well samples typically shows more porosity in the organic matter (Mathia et al., 2016). Comparing these results to results of typical US gas shales (Loucks et al., 2012; Klaver et al., 2015a) shows that the PSF/WMF samples investigated here are similar, regarding number of pores in matrix/organic matter/other pores, to the Haynesville, Bossier, Pearsall and Pliocene/Pleistocene mudstones, whereas the Barnett shale shows typically mostly pores in the organic matter (Loucks et al., 2012).

5.3. Microstructure

Typical shale microstructures, where silt sized particles and fossils are embedded within a fine-grained matrix (Fig. 3; e.g. Curtis et al., 2012), are found in samples originating from the basin edge. WMF samples can be microstructurally subdivided in a calcite fossil rich upper half and a calcite (fossil) poor lower half (Zijp et al., 2015; Houben

Fig. 4. Graphs showing box size in micrometer on the x-axis and percentage in percent on the y-axis. In graphs a.–c. information about the percentage of amount of matrix can be found, d.–f. show the percentage of minerals present, g.–i. show the percentage of organic matter and j.–l. show the pyrite content present.

Table 1
Visible SEM porosity of the PIPS polished samples, and mineralogy in Area% as encountered in the PIPS and mechanically polished SEM samples using a combination of BSE images and EDX measurements. Calculations were made for the whole imaged high resolution mosaic, meaning a box size of >300 × 300 μm. PIPS stands for Precision Ion Polished samples and TH refers to the mechanically polished thin section samples. Relative variabilities per mineral phase can be found at the top of the table to get an idea of the variability from an area size of 150 × 150 μn onwards.

Polishing method	Sample	Geographical location	Mosaic	Depth (m)	Total visible SEMφ (area%)	Matrix ±0.44%	Silicates ±1.60%	Carbonates ±1.60%	Sulfides ±1.18%	Organic matter ±1.38%
PIPS	PSF-L51	Dutch Central Graben	1	−2824.0	0.7	30.1	0.0	50.7	2.3	16.9
PIPS	PSF-L51	Dutch Central Graben	2	−2824.0	0.6	31.3	0.0	54.8	2.7	11.2
PIPS	PSF-L53	Dutch Central Graben	1	−2826.0	0.3	34.7	0.7	23.8	3.2	37.5
TH	PSF-L5-S22	Dutch Central Graben	1	−2826.5	–	71.3	1.3	15.1	3.8	8.5
TH	PSF-L5-S23	Dutch Central Graben	1	−2827.4	–	70.3	2.7	6.3	3.0	17.8
TH	PSF-L5-S23	Dutch Central Graben	2	−2827.4	–	75.4	2.2	4.4	2.7	15.4
TH	PSF-L5-S24	Dutch Central Graben	1	−2829.5	–	77.7	2.7	2.1	5.0	12.5
TH	PSF-L5-S24	Dutch Central Graben	2	−2829.5	–	76.3	3.6	2.5	4.1	13.6
TH	PSF-L5-S25	Dutch Central Graben	1	−2831.8	–	55.1	2.0	36.8	2.0	4.2
PIPS	PSF-l5-5	Dutch Central Graben	1	−2832.0	0.3	45.1	0.9	47.1	2.6	4.2
PIPS	PSF-l5-5	Dutch Central Graben	2	−2832.0	0.3	42.8	0.3	47.9	2.6	6.4
PIPS	PSF-l5-5	Dutch Central Graben	3	−2832.0	0.6	38.0	0.1	53.1	1.9	6.9
TH	PSF-L5-S26	Dutch Central Graben	1	−2832.8	–	78.4	1.1	1.7	1.5	17.3
TH	PSF-L5-S27	Dutch Central Graben	1	−2833.7	–	72.7	1.2	9.7	4.0	12.4
TH	PSF-L5-S27	Dutch Central Graben	2	−2833.7	–	67.9	0.9	16.1	1.4	13.7
PIPS	PSF-l5-8	Dutch Central Graben	1	−2834.0	1.3	67.6	2.2	17.8	5.3	7.1
PIPS	PSF-l5-8	Dutch Central Graben	2	−2834.0	0.9	64.6	1.2	16.0	4.6	13.6
TH	PSF-L5-S28	Dutch Central Graben	1	−2836.5	–	78.1	3.0	0.2	3.3	15.3
TH	PSF-L5-S29	Dutch Central Graben	1	−2837.5	–	76.0	1.2	0.5	1.5	20.7
TH	PSF-L5-S29	Dutch Central Graben	2	−2837.5	–	75.1	1.0	1.5	1.7	20.7
TH	PSF-L5-S31	Dutch Central Graben	1	−2839.2	–	85.0	0.8	0.0	1.4	12.8
TH	PSF-L5-S31	Dutch Central Graben	2	−2839.2	–	74.9	3.7	0.1	2.0	19.3
PIPS	WMF4	Runswick Bay (UK)	1	5.5	1.9	59.5	3.1	27.5	3.6	6.3
PIPS	WMF4	Runswick Bay (UK)	2	5.5	1.8	64.5	3.1	19.4	3.8	9.2
PIPS	WMF4	Runswick Bay (UK)	3	5.5	1.4	70.5	3.3	16.4	3.5	6.4
PIPS	WMF6	Runswick Bay (UK)	1	4.2	–	66.9	3.2	19.3	4.4	6.1
PIPS	WMF6	Runswick Bay (UK)	2	4.2	0.5	63.2	3.5	20.8	4.0	8.4
PIPS	WMF15a	Port Mulgrave (UK)	1	2.7	1.4	71.2	15.9	3.0	2.8	7.1
PIPS	WMF15a	Port Mulgrave (UK)	2	2.7	2.3	73.7	13.1	10.3	2.5	0.3
PIPS	WMF15a	Port Mulgrave (UK)	3	2.7	2.5	72.4	5.6	1.4	4.8	15.7
PIPS	WMF15b	Port Mulgrave (UK)	1	2.7	1.3	71.8	8.8	3.4	4.8	11.2
PIPS	WMF15b	Port Mulgrave (UK)	2	2.7	–	76.9	9.7	1.2	4.4	7.8
PIPS	WMF1	Runswick Bay (UK)	2	1.0	0.9	66.7	19.0	9.5	3.6	1.2
PIPS	WMF1	Runswick Bay (UK)	3	1.0	0.6	77.2	10.4	3.1	4.4	5.0
PIPS	WMF1	Runswick Bay (UK)	4	1.0	0.9	71.9	12.7	5.9	5.0	4.4
PIPS	WMF23	Port Mulgrave (UK)	1	0.0	1.0	76.0	9.9	3.5	3.7	6.9
PIPS	WMF23	Port Mulgrave (UK)	2	0.0	–	74.1	8.4	4.2	3.4	9.9
PIPS	WMF23	Port Mulgrave (UK)	3	0.0	0.9	78.5	7.4	2.9	3.9	7.3
PIPS	LOZ-S37	Loon op Zand (NL)	2	−2495.0	0.8	63.0	1.9	6.1	4.3	24.8
PIPS	LOZ-S37	Loon op Zand (NL)	20	−2495.0	0.8	51.4	2.4	11.4	3.4	31.4
PIPS	LOZ-S37	Loon op Zand (NL)	21	−2495.0	1.1	63.8	1.6	12.5	3.6	18.5
PIPS	LOZ-S37	Loon op Zand (NL)	22	−2495.0	1.0	61.7	3.3	10.8	3.3	21.0
PIPS	LOZ-S41	Loon op Zand (NL)	2	−2507.0	1.8	67.3	5.4	9.5	2.1	15.7
PIPS	LOZ-S41	Loon op Zand (NL)	3	−2507.0	0.9	72.8	5.9	11.1	2.6	7.6
PIPS	LOZ-S41	Loon op Zand (NL)	5	−2507.0	0.7	65.4	6.7	11.8	4.0	12.0
PIPS	LOZ-S41	Loon op Zand (NL)	7	−2507.0	0.6	71.5	4.9	10.0	3.5	10.0
PIPS	LOZ-S41	Loon op Zand (NL)	9	−2507.0	0.5	75.3	5.2	9.7	2.8	7.0
PIPS	PSF-D1	Dotternhausen (DE)	1	0.5	1.0	56.8	4.2	18.9	1.5	18.6
PIPS	PSF-D1	Dotternhausen (DE)	5	0.5	–	55.7	3.2	25.1	1.7	14.3
TH	PSF-F11S11	Dutch Central Graben	1	−2658.0	–	73.2	1.4	13.9	3.8	7.7
TH	PSF-F11S12	Dutch Central Graben	1	−2659.0	–	24.8	6.9	58.6	3.2	6.5
TH	PSF-F11S14	Dutch Central Graben	1	−2661.0	–	64.6	12.2	4.0	4.7	14.5
TH	PSF-F11S15	Dutch Central Graben	1	−2662.0	–	72.4	6.3	1.1	4.8	15.3
TH	PSF-F11S17	Dutch Central Graben	1	−2665.0	–	75.1	6.2	3.1	1.9	13.7
TH	PSF-F11S18	Dutch Central Graben	1	−2666.0	–	82.0	3.4	0.1	3.4	11.0
TH	PSF-F11S18	Dutch Central Graben	2	−2666.0	–	81.5	5.6	0.3	2.0	10.6
TH	PSF-F11S39	Dutch Central Graben	1	−2669.0	–	87.6	4.5	1.9	1.5	4.5
TH	PSF-F11S41	Dutch Central Graben	1	−2671.0	–	88.6	2.9	0.4	2.7	5.3
TH	PSF-F11S41	Dutch Central Graben	2	−2671.0	–	84.8	2.7	3.4	2.2	6.9
TH	PSF-F11S42	Dutch Central Graben	1	−2672.0	–	81.3	4.5	3.0	2.2	9.0

et al., 2016). Microstructures in the upper half of the WMF section (WMF4, WMF6) are dominated by porous calcite fossil and similar calcite fossils were found in PSF-LOZ, PSF-D and in PSF-Hils (Bernard et al., 2012; Klaver et al., 2012) samples. The organic matter content (identified in the SEM images) is on average circa 7 area% for samples from the WMF section and averaging 13 area% for the PSF samples (PSF-L5, PSF-LOZ, PSF-D, PSF-Hils; Klaver et al., 2012). Published TOC data (Zijp et al., 2015) shows a similar trend as we found in the WMF section of an increase of TOC/organic matter towards the Whalestones and a decrease from the Whalestones to the bottom of the section. Furthermore, Zijp et al. (2015) confirm that TOC values at Runswick Bay (WMF) are slightly lower (3–4 wt%) than the TOC values in the Meerkerk-01 well (6–8 wt%, where the Meerkerk well is comparable to the PSF-LOZ well). Saelen et al. (2000) show TOC values for the WMF in the range from 0.7 to 16.4 wt% (again with a local high around the Whalestones) and on average TOC is about 6 wt%. PSF-D shows TOC values ranging

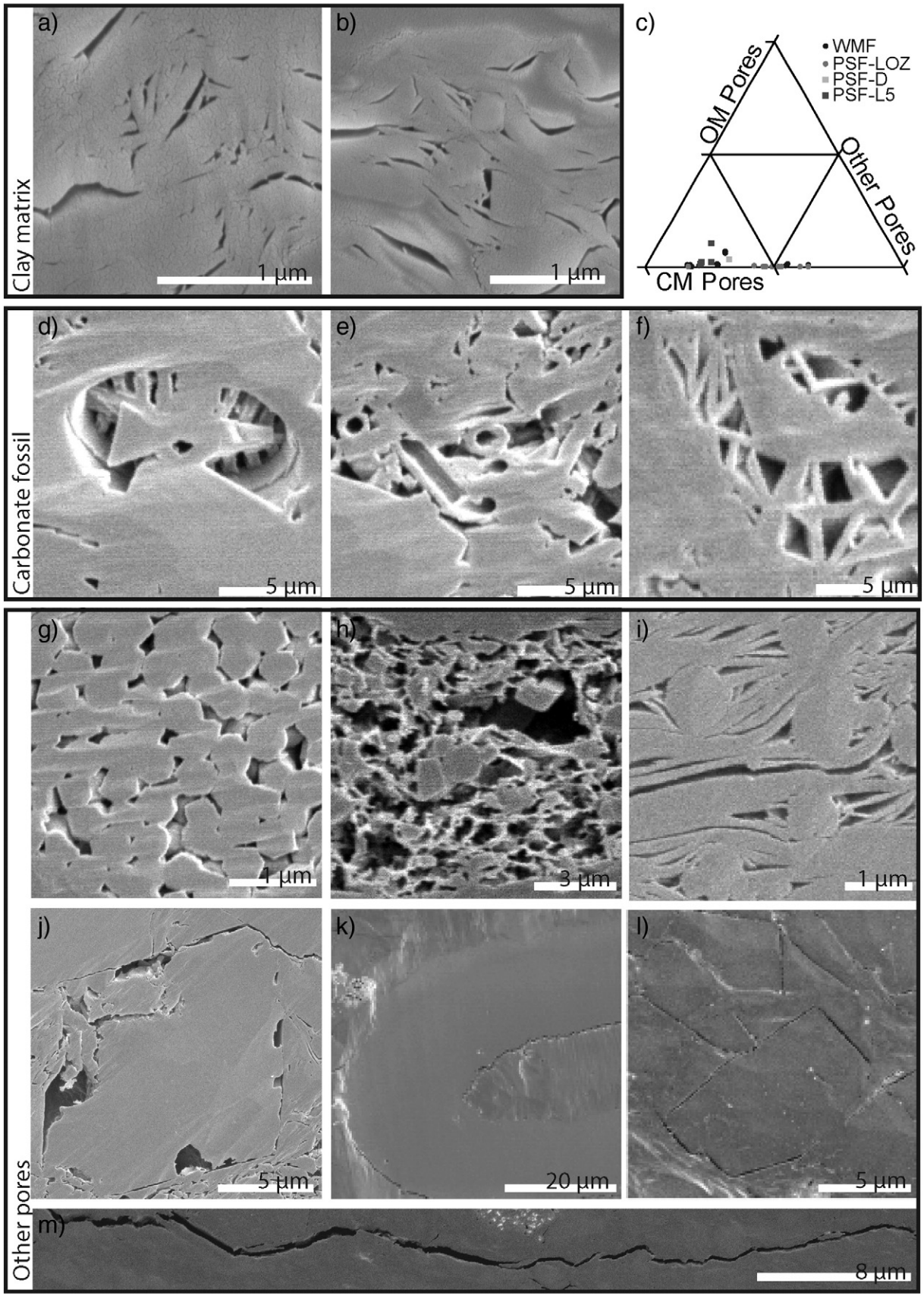

Fig. 5. Pores in different minerals/mineral aggregates encountered in the PIPS-SEM samples investigated. a.–b. Pores situated in the matrix. c. Ternary diagram of pores encountered in organic matter (OM Pores), matrix (CM Pores) and other minerals/mineral aggregates (Other Pores). d.–f. Pores in porous calcareous fossils. g. Pores in framboidal pyrite. h. Pores in organic matter. i. Pores in mica. j. Dissolution pores surrounding mineral. k. Cracks surrounding organic matter. l. Cracks surrounding mineral. m. Typical drying/stress relaxation crack running through the matrix.

Table 2
Mineralogy in weight (%) based on the XRD results for the Whitby Mudstone (UK) and Posidonia Shale (LOZ, NL) samples for both bulk rock measurements and clay fraction measurements.

			Sheetsilicates (Bulk)			Silicates		Carbonates			Sulfides	Sulfates	Sheetsilicates (Clay fraction)			
Sample	Height	No.	2:1 Al/Fe sheetsilicates	Kaolinite	Chlorite	Quartz	Plagioclase	Calcite	Ankerite	Anatase	Pyrite	Gypsum	Illite 80/Smectite 20	Illite	Kaolinite	Chlorite
WMF	5.5	4[a]	38.1	11.5	1.7	13.1	0.0	25.1	1.0	0.6	7.7	0.9	54	17	26	3
	4.2	6[a]	40.4	15.1	3.9	15.2	0.7	12.0	0.1	0.6	11.0	0.7	31	27	39	4
	2.7	15[a]	42.1	23.5	2.8	16.3	1.0	1.7	2.8	0.9	8.0	0.0	42	17	38	3
	1	1[a]	43.9	22.6	3.4	16.0	0.9	1.3	1.7	0.7	8.5	0.0	38	19	40	3
PSF-LOZ	-2481	32	29.8	17.5	2.3	15.3	2.9	20.1	0.6	0.6	5.8	1.5	38	24	33	1
	-2484	33	30.2	17	3.7	14.9	2.7	19	1.4	1.3	5.6	1.2	24	29	45	1
	-2485	34	22.1	15.9	1.9	13.1	2.1	34.1	0.7	0.7	4.9	2.0	37	22	39	2
	-2487	35	25.5	13.2	1.8	12.8	2.6	24.6	8.1	1	5.4	1.5	42	27	30	1
	-2489	36	16.5	8.1	1.3	12.9	1.5	44.9	5.3	0.4	3.8	2.8	27	32	39	2
	-2495	37	28	12.1	2.5	13.7	2.5	26.4	1.1	0.9	7.7	3.5	39	27	34	1
	-2497	38	28.4	16.9	3	14	2.2	16.9	0.8	1.3	9.4	4.0	39	28	33	1
	-2499	39	26.9	12.9	3.1	30.5	3.1	7.3	1.9	1	6.4	1.7	31	46	21	2
	-2503	40	24.8	11.3	3.7	17.8	3.3	14.8	11.6	1	7.3	1.5	38	37	23	2
	-2507	41	30.3	14.6	4.4	18.3	4.3	7.7	6.4	1.3	6.4	1.7	36	33	26	5

[a] Houben et al. (2016).

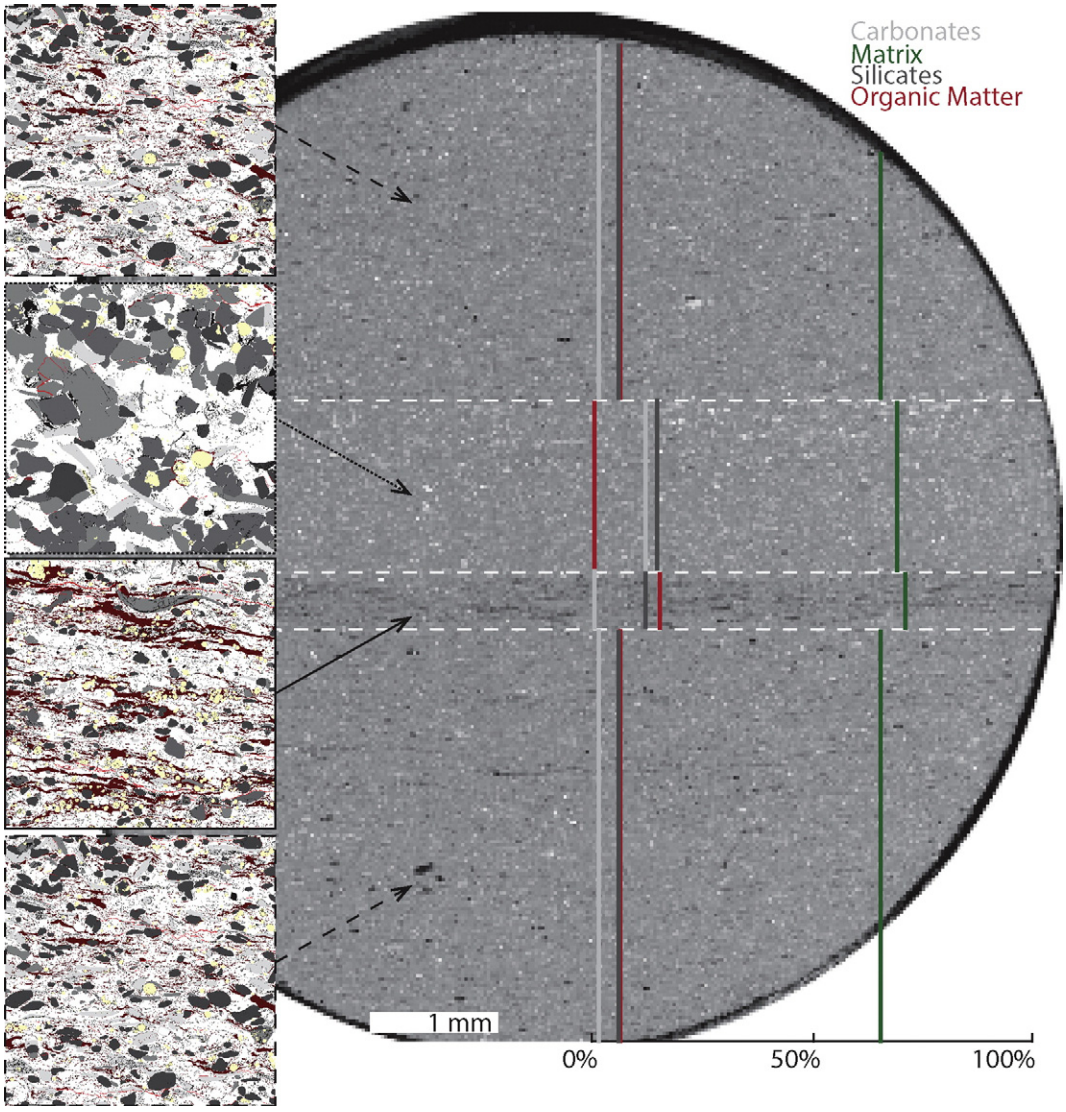

Fig. 6. PIPS-SEM sample WMF15a with the microstructure found in the different mineralogical layers within the sample to the left, and the mineralogy per layer based on the SEM measurements. When knowing the microstructure within a certain layer, the data can be extrapolated to upscale the PIPS-SEM information up to the cm scale.

from 2 to 16 wt% (Röhl et al., 2001) with an average TOC value around 6 wt%, PSF-Hils samples show TOC values between 4 and 11 wt% (Bernard et al., 2012; Klaver et al., 2012; Klaver et al., 2016), PSF-L5 shows TOC values in the range from 2 to 20 wt% (Trabucho-Alexandre et al., 2012) and TOC values for PSF-F11 range between 2 and 15 wt% (Trabucho-Alexandre et al., 2012) with an average value of 9 wt%. Hence TOC values show a similar trend as the PIPS-SEM organic matter data, TOC values overlap in the WMF and PSF samples where the samples from the Hils Area and Dotternhausen on average show slightly higher TOC and organic matter values. Pyrite (mainly framboidal pyrite) is evenly spread and found scattered throughout all PSF/WMF samples (see also: Bernard et al., 2012; Kanitpanyacharoen et al., 2012; Klaver et al., 2012; Trabucho-Alexandre et al., 2012).

5.4. Mineralogy

XRD results (Kanitpanyacharoen et al., 2012; Klaver et al., 2012, 2016; Gasparik et al., 2014; Ghanizadeh et al., 2014; Hilger, 2003; Rexer et al., 2014) show that the carbonate content is higher for the German PSF samples (20–70 wt%) than for the WMF samples (3–27 wt%)

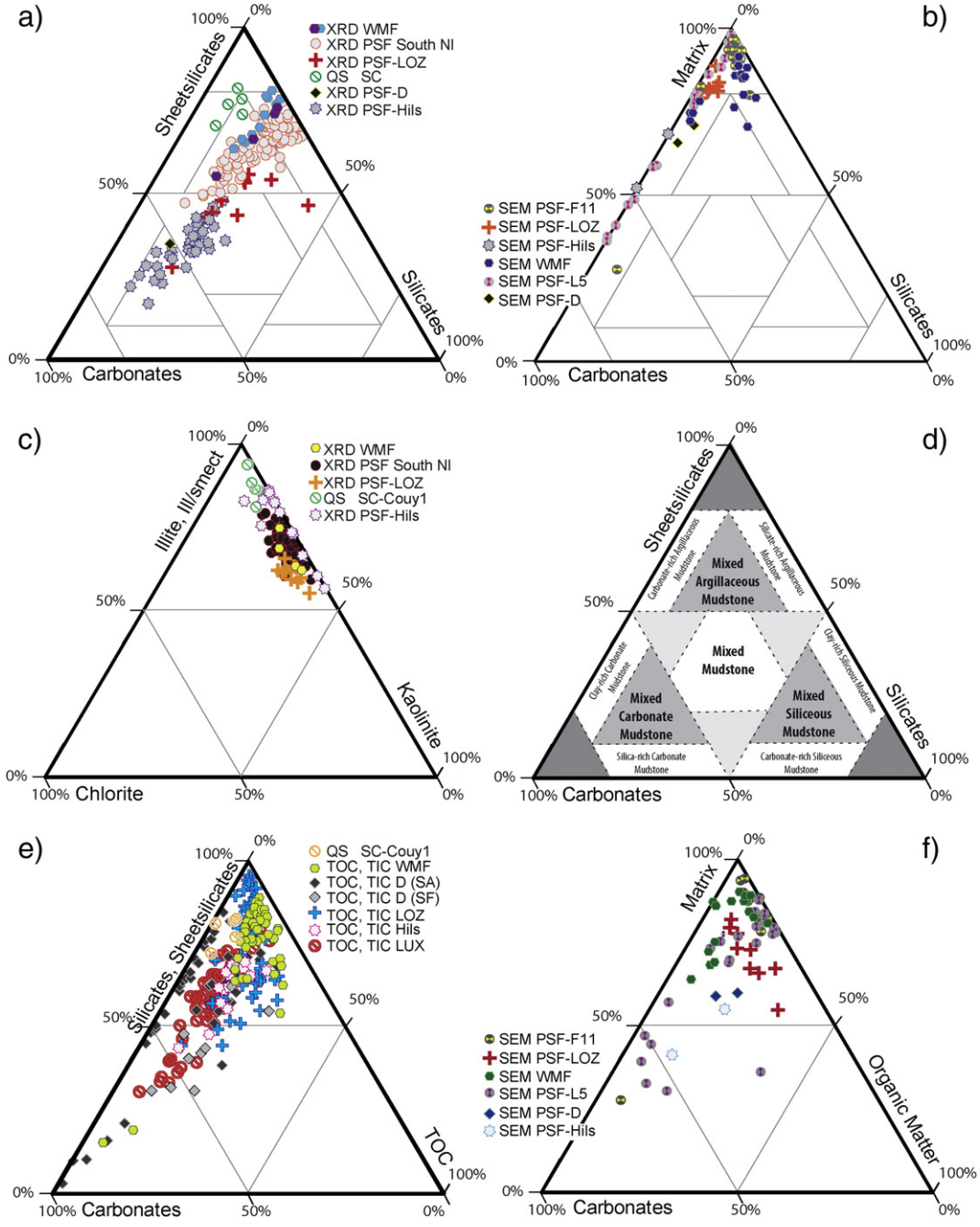

Fig. 7. Ternary diagrams summarizing the mineralogy of the samples in wt%. a. XRD measurements summarizing the sheetsilicate, silicate and carbonate contents of WMF and PSF samples. WMF data after Houben et al. (2016), PSF-SouthNL data after Chesapeake (2010), SC-Couy1 data after Power et al. (2014), PSF-D data after Hilger (2003), and PSF-Hils data after Klaver et al. (2012, 2016); Kanitpanyacharoen et al. (2012); Gasparik et al. (2014); Ghanizadeh et al. (2014); Rexer et al. (2014) and Mathia et al. (2016). b. Mineralogy based on the SEM BSE images summarizing the sheetsilicate, silicate and carbonate contents of the different samples. PSF-Hils data after Klaver et al. (2012), SC-Couy1 data after Power et al. (2014) c. XRD measurement summarizing the clay mineralogy. WMF data after Houben et al. (2016), PSF-SouthNL data after Chesapeake (2010), SC-Couy1 data after Power et al. (2014), PSF-Hils data after Klaver et al. (2012, 2016); Kanitpanyacharoen et al. (2012); Rexer et al. (2014). d. Mudstone classification after Diaz et al. (2014). e. Silicates/sheetsilicates, versus carbonates and TOC after Song et al. (2014, 2015). f. Organic matter, matrix and carbonate content based on the SEM. Data from the PSF-Hils samples after Klaver et al. (2012) and SC-Couy1 data after Power et al. (2014).

and the PSF samples originating from the South of the Netherlands (PSF-SouthNL; Chesapeake, 2010; Fig. 7a). This difference is not so clear from the SEM data, although the PSF-Hils (Klaver et al., 2012), PSF-L5 and PSF-F11 samples do show carbonate contents in some layers that are on the high end, whereas on average the WMF, Schistes Carton (SC) and PSF-LOZ samples show lower carbonate contents (Fig. 7b). Most samples plot in the mixed argillaceous mudstone, mixed carbonate mudstone and the mixed mudstone ranges (after Diaz et al., 2014; Fig. 7a–d). The XRD silicate contents (mainly quartz) are between 20 and 25 wt% for all samples and this is similar to values found in literature for PSF samples (Kanitpanyacharoen et al., 2012; Klaver et al., 2012, 2016; Gasparik et al., 2014; Ghanizadeh et al., 2014; Hilger, 2003; Rexer et al., 2014). QEMSCAN results for the Schistes Carton (Power et al., 2014) show slightly lower quartz contents (10–15 wt%) than found for the XRD values of the WMF/PSF samples. Mineralogical differences could have been caused by difference in mineral content but can also be due to methodological differences between the measuring methods (XRD versus QEMSCAN versus SEM; Power and Burns, 2013). Since the discrepancy between the QEMSCAN and XRD results is similar to the one found between the XRD and the SEM/EDX methods described in the Representative Elementary Area section of the discussion, it is clear that method also plays an important role and that based on the data we cannot distinguish whether the different values represent real mineralogical differences or are due to methodological differences. Comparing the XRD PSF/WMF mineralogy to mineralogy of other known gas shales shows that the PSF/WMF samples plot on the silicate poor end of the diagram and that mineralogically the PSF/WMF samples are most similar to the Haynesville shale (e.g.: Jarvie et al., 2007; Chalmers et al., 2012; Curtis et al., 2012; Gasparik et al., 2014; Klaver et al., 2015a; Houben et al., 2016).

The mineralogical brittleness index (BI; Curtis, 2002; Jarvie et al., 2007; Wang and Gale, 2009) can be used to get an indication of the brittle versus ductile behaviour of the shales, although the use of shale brittleness index based on just the mineralogy is poorly defined (Yang et al., 2013). The mineralogical BI's for the PSF/WMF vary between 0.1 and 0.4 with an average value around 0.2 (WMF – 0.18, PSF-HA – 0.19, PSF-LOZ – 0.24, PSF-SouthNL – 0.21, PSF-D – 0.14, SC – 0.11), meaning that we are dealing with shales in a ductile to less ductile regime (Perez Altamar and Marfurt, 2015). Ter Heege et al. (2015) found similar values for the PSF in the southern part of the Netherlands (0.14–0.23) and Houben et al. (2016) show a mineralogical BI <0.2 for WMF samples. In addition, WMF/PSF mineralogical BI values are most similar to the US Marcellus shale (Mineralogical BI 0.1–0.6; ter Heege et al., 2015), where other US shale formations show higher mineralogical BI values (Bakken – 0.2-0.8; Haynesville – 0.3-0.7; Barnett – 0.4-0.8; ter Heege et al., 2015). These results could point towards more ductile behaviour of the PSF/WMF samples and less favourable behaviour with respect to mechanical fracturing of these rocks, although this mineral BI should still be combined with elastic parameters or shale mechanical behaviour to give a better prediction of fracturing behaviour (Yang et al., 2013; Holt et al., 2015; ter Heege et al., 2015; Houben et al., 2016; Meier and Dresen, 2016).

Clay mineralogy measured of WMF, PSF and SC samples is similar for all samples (Fig. 7c), most different are again the QEMSCAN measured samples (SC). Comparing these results to US-gas shales shows that the US-gas shales are more illite and less kaolinite rich than the PSF/WMF samples (Chalmers et al., 2012). PSF/WMF samples investigated in this study show very little swelling clays (e.g.: smectite), smectite is only present interlayered with illite where the illite/smectite ratio is 80/20 respectively meaning that smectite accounts for about 3% of the total mineralogy. According to literature (Kemp et al., 2005; Imber et al., 2014) the WMF found at coastal outcrops North of Whitby have had a maximum burial depth of 2–4 km which is reflected in the high illite content of the rock. Kemp et al. (2005) found 90% of illite present in the interlayered illite/smectite layers of the Cleveland Basin (which is slightly higher than the 80% we found in this study), which suggest a maximum burial depth of 4 km, furthermore they mention an R_0 of 0.85 (oil mature). Saelen et al. (2000) report a burial depth between 2.2 and 2.5 km and an R_0 between 0.55 and 0.65 (low mature; Raiswell et al., 1993) for the WMF. These vitrinite reflectance values are comparable to the maturity found in PSF-HA samples of the Wickensen and Harderode wells (Bernard et al., 2012; Klaver et al., 2012), whereas the Haddessen well shows an R_0 of 1.45 (overmature; Bernard et al., 2012). In addition, illite/smectite content is comparable for all samples confirming that samples throughout the basin have experienced similar maximal burial depths.

One can find a plot of the carbonate versus silicate/sheetsilicate versus organic matter content for PSF/WMF samples as observed by Song et al. (2014, 2015) in Fig. 7e, where a temperature ramp method was used to determine the Total Organic Carbon (TOC) and the Total Inorganic Carbon (TIC) contents. A similar plot can be made for the carbonate versus matrix versus organic matter content as present in the SEM mosaics (Fig. 7f), where the results can be qualitatively compared to data published by Song et al. (2014, 2015). Comparing Figs. 7e and f shows that most of the data plot in the matrix and silicates/sheetsilicates high end (> 50%) and display an organic matter content below 30% with a minor amount of the samples being more carbonate rich for both the SEM and TOC/TIC data. Regional variability is not much higher than the variability present in samples originating from one location (Fig. 8), where the SEM data is recalculated to represent wt% using density values for the matrix, silicates, carbonates and organic matter contents of respectively: 2.68, 2.65, 2.71 and 1.1 g/m^3. Most of the samples show a spread in the carbonate content data that is directly related to the amount of matrix/sheetsilicates present. There is a clear two fold in carbonate content in the PSF-L5 and PSF-F11 samples showing either carbonate rich or carbonate poor layers (Fig. 7b, f). The data is most scattered for the PSF-D samples (Fig. 8e, f), covering the whole range of carbonate contents. The PSF-HA (Fig. 8g, h) are overall on average more carbonate rich, whereas the PSF-LOZ (Fig. 8c, d) and WMF (Fig. 8a,b) samples are more carbonate poor. Organic matter content is variable in all samples and is ranging from zero to about almost 40% (Fig. 8), where the largest spread is found in the PSF-LOZ samples followed by the WMF, PSF-D and PSF-HA samples.

Most data points towards low maturity of the WMF and PSF samples investigated here, where most of the investigated samples show similar SEM microstructures typical for mudstones. Samples fall within the argillaceous/carbonate/mixed mudstone ranges and the largest variation was found in the carbonate content that varies between the PSF-D (outcrop), PSF-HA (core), PSF-LOZ (core) samples on the one end and the PSF-SouthNL (core), WMF (outcrop) and SC (core) on the other end, with the PSF-L5 and PSF-F11 showing alternation of carbonate rich and carbonate poor layers. The variations in carbonate content probably reflect a difference in sediment source, diagenesis or depositional environment, but there is no evidence found that the outcrop samples

Fig. 8. XRD, SEM and TOC/TIC data per location. a. Sheetsilicates versus Silicates versus Carbonates for the WMF samples. WMF XRD data after Houben et al. (2016). b. Matrix versus Organic Matter versus Carbonate for the WMF samples. TOC/TIC data after Song et al. (2015). c. Sheetsilicates versus Silicates versus Carbonates for the PSF-LOZ samples. XRD PSF-SouthNL data after chesapeake (2010). d. Matrix versus Organic Matter versus Carbonate for the PSF-LOZ samples. XRD/TOC data after Chesapeake (2010) and TOC/TIC data after Song et al. (2015). e. Sheetsilicates versus Silicates versus Carbonates for the PSF-D samples. XRD PSF-D data after Hilger (2003). f. Matrix versus Organic Matter versus Carbonate for the PSF-D samples. TOC/TIC data after Song et al. (2015). g. Sheetsilicates versus Silicates versus Carbonates for the PSF-Hils samples. SEM data after Klaver et al. (2012) and XRD data after Klaver et al. (2012, 2016); Kanitpanyacharoen et al. (2012); Gasparik et al. (2014); Ghanizadeh et al. (2014); Rexer et al. (2014) and Mathia et al. (2016). h. Matrix versus Organic Matter versus Carbonate for the PSF-Hils samples. SEM data after Klaver et al. (2012), XRD/TOC data after Klaver et al. (2012, 2016); Kanitpanyacharoen et al. (2012); Gasparik et al. (2014); Ghanizadeh et al. (2014); Rexer et al. (2014) and Mathia et al. (2016), and TOC/TIC data after Song et al. (2015).

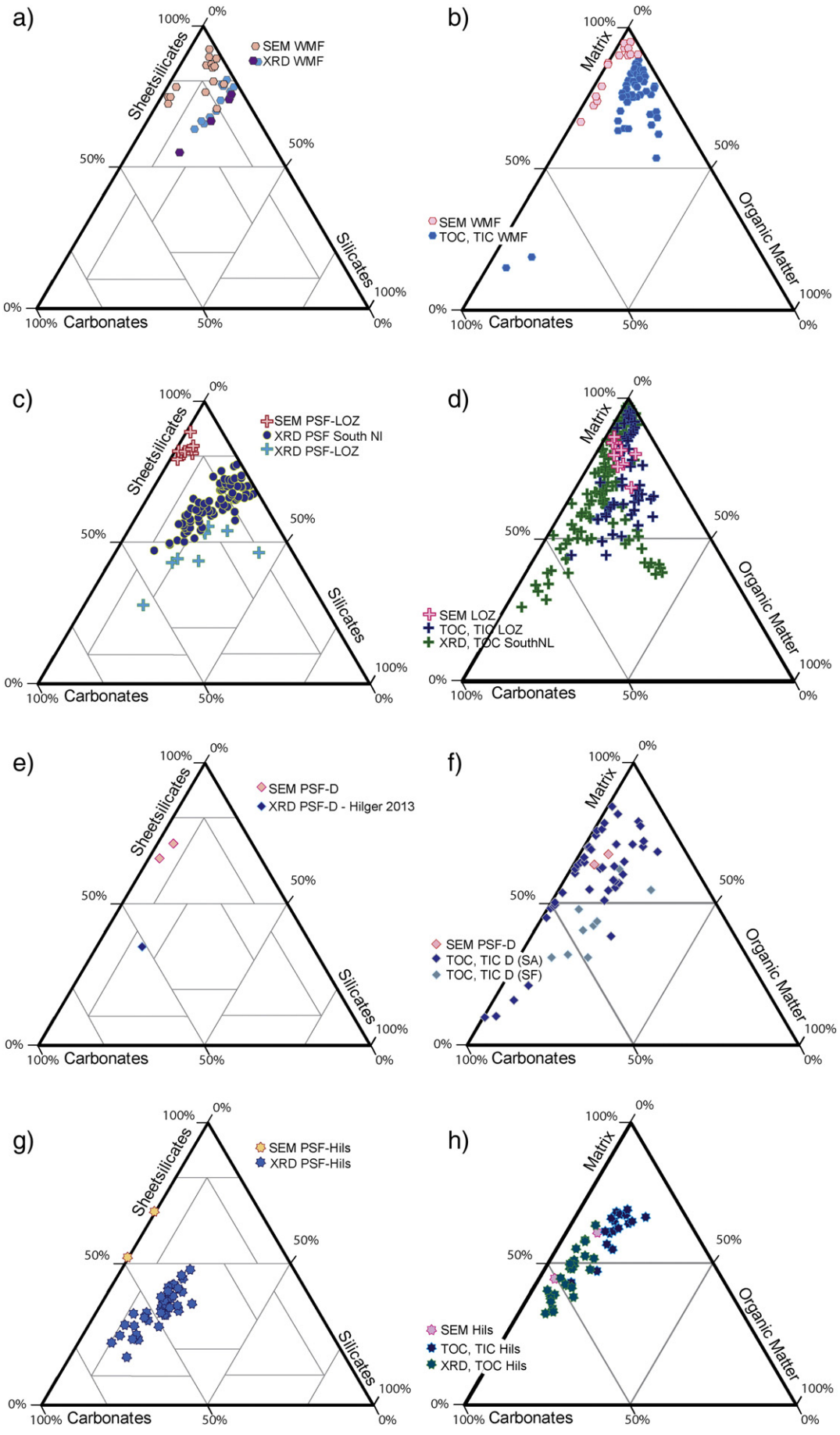
a)
Sheetsilicates
Carbonates
Silicates
SEM WMF
XRD WMF
b)
Matrix
Carbonates
Organic Matter
SEM WMF
TOC, TIC WMF
c)
Sheetsilicates
Carbonates
Silicates
SEM PSF-LOZ
XRD PSF South NI
XRD PSF-LOZ
d)
Matrix
Carbonates
Organic Matter
SEM LOZ
TOC, TIC LOZ
XRD, TOC SouthNL
e)
Sheetsilicates
Carbonates
Silicates
SEM PSF-D
XRD PSF-D - Hilger 2013
f)
Matrix
Carbonates
Organic Matter
SEM PSF-D
TOC, TIC D (SA)
TOC, TIC D (SF)
g)
Sheetsilicates
Carbonates
Silicates
SEM PSF-Hils
XRD PSF-Hils
h)
Matrix
Carbonates
Organic Matter
SEM Hils
TOC, TIC Hils
XRD, TOC Hils

cannot be used for experimental studies one just has to test the mineralogical composition beforehand to check whether we are dealing with a carbonate rich sample or a carbonate poor end-member.

6. Conclusions

PSF/WMF samples display typical shale microstructures, where silt-sized grains with diameters <20 μm (mainly quartz, carbonates (fossils, calcite, dolomite) and pyrite) are embedded within a fine grained matrix. In all samples organic matter is present interlayered with the matrix and contents run up to about 40% in some samples, but on average we found an organic matter content of 15%. Quartz content is homogeneous throughout the different samples (ca. 20% based on XRD measurements) whereas the carbonate content varies per location in the basin and height in the section. Visible porosity in the SEM mosaics is in the order of 0.3–2.5% and most of the porosity is situated in the matrix. Highly porous are the carbonate fossils with porosities up to 11%, were the occurrence of the fossils is not influencing fluid migration through the rock since the fossils are not forming a connected pore network.

Overall the lower Toarcian deposits in Germany, The Netherlands and the UK show similar microstructures confirming the suggestion of similar depositional environments during deposition. Samples from some of the locations (PSF-D, PSF-HA, PSF-LOZ) fall within the carbonate rich mudstone range whereas the PSF-SouthNL, WMF and SC fall within the argillaceous rich mudstone range. In addition, samples from the North Sea (PSF-F11, PSF-L5) show alternating more argillaceous and more carbonate rich mudstone layers, lacking the mixed mudstone microstructures. All investigated samples could be used for experiments there was no evidence found that outcrop samples are microstructurally more altered than core samples, but since usually cm-sized samples have to be used one has to make the samples long enough to be representative also when mm-scaled layers are present within the sample.

Acknowledgements

We would like to thank T. van de Gon Netscher for modifying SEM stubs so that they fitted the PIPS. P. van Krieken is thanked for drilling 8 mm cores from the sample blocks. R. van Noort and L. Buijze are thanked for gathering sample material in Dotternhausen and providing the material for this project. Engie is acknowledged for providing the L05-4 samples. F. van der Goes is thanked for doing PIPS-SEM, XRD and XRF method tests on PSF-LOZ sample material. Collaboration with TNO during the WMF sampling campaign was greatly appreciated, as well as funding by the Topsector Energy Innovation Program (TKIG01017) upstream gas and our industry partners: EBN, Engie, Wintershall, Total and Baker Hughes. This paper benefited greatly from the thorough reviews of two anonymous reviewers.

References

Bernard, S., Horsfield, B., Schulz, H.-M., Wirth, R., Schreiber, A., Sherwood, N., 2012. Geochemical evolution of organic-rich shales with increasing maturity: a STXM and TEM study of the Posidonia Shale (Lower Toarcian, northern Germany). Mar. Pet. Geol. 31, 70–89.

Chalmers, G.R.L., Ross, D.J.K., Bustin, R.M., 2012. Gelogical controls on matrix permability of Devonian gas Shales in the Horn rinver and Liard Basins, northeastern Britisch Columbia, Canada. Int. J. Coal Geol. 103, 120–131.

Chesapeake, 2010. Posidonia Cutting Research, 26th of July 2010. available through www.nlog.nl.

Curtis, J.V., 2002. Fractured shale-gas systems. AAPG Bull. 86 (11), 1921–1938.

Curtis, M.E., Sondergeld, C.H., Ambrose, R.J., Rai, C.S., 2012. Microstructural investigation of gas shales in two and three dimensions using nanometer-scale resolution imaging. AAPG Bull. 96 (4), 665–677.

De Jager, J., Doyle, M.A., Granham, P.J., Mabillard, J.E., 1996. Hydrocarbon habitat of the West Netherlands Basin. In: Rondeel, H.E., Batjes, D.A.J., Nieuwenhuijs, W.H. (Eds.), Geology of Gas and Oil Under the Netherlands. Kluwer, Dordrecht, pp. 191–209.

Desbois, G., Urai, J.L., Kukla, P.A., 2009. Morphology of the pore space in claystones - evidence from BIB/FIB ion beam sectioning and cryo-SEM observations. eEarth 4, 15–22.

Desbois, G., Urai, J.L., Houben, M., Hemes, S., Klaver, J., 2011. BIB-SEM of representative area clay structures: insights and challenges. NEA ClayClub Workshop Proceedings – Clays Under Nano- to Microscopic Resolution, Karlsruhe (Germany), 6–8 September 2011.

Diaz, H.G., Fuentes, C.C., Calvin, C., Yang, Y., MacPhail, K., Lewis, R., 2014. Evaluating the impact of mineralogy on reservoir quality and completion quality of organic shale plays. AAP G Datapages, 90228, GTW Marcellus and Utica Point Pleassant, Pittsburgh, Pennsylvania, p. 6.

Emmanuel, L., Renard, M., Cubaynes, R., De Rafelis, M., Hermoso, M., Lecallonnec, L., Le Solleuz, A., Rey, J., 2006. The "Schistes Carton" of Quercy (Tarn, France): a lithological signature of a methane hydrate dissociation event in the early Toarcia. Implications for correlations between Boreal and Tethyan realms. Bull. Soc. geol. Fr., t. 177 (5), pp. 239–249.

French, K.L., Sepúlveda, J., Trabucho-Alexandre, J., Gröcke, D.R., Summons, R.E., 2014. Organic geochemistry of the Early Toarcian oceanic anoxic event in Hawsker Bottoms, Yorkshire, England. Earth Planet. Sci. Lett. 390, 116–127.

Gasparik, M., Bertier, P., Gensterblum, Y., Ghanizadeh, A., Krooss, B.M., Littke, R., 2014. Geological controls on the methane storage capacity in organic-rich shales. Int. J. Coal Geol. 123, 34–51.

Ghanizadeh, A., Gasparik, M., Amann-Hildenbrand, A., Gensterblum, Y., Krooss, B.M., Littke, R., 2014. Experimental study of fluid transport processes in the matrix system of the European organic-rich shales: II Posidonia Shale. Int. J. Coal Geol. 123, 20–33.

Hemes, S., Desbois, G., Urai, J.L., De Craen, M., Honty, M., 2013. Variations in the morphology of porosity in the Boom Clay Formation: insights from 2D high resolution BIB-SEM imaging and mercury injection porosimetry. Neth. J. Geosci. 92-4, 275–300.

Hemes, S., Desbois, G., Urai, J.L., Schröppel, B., Schwarz, J.-O., 2015. Multi-scale characterization of porosity in Boom Clay (HADES-lever, Mol, Belgium) using a combination of X-ray μ-CT, 2D BIB-SEM and FIB-SEM tomography. Microporous Mesoporous Mater. 208, 1–20.

Herber, R., de Jager, J., 2010. Oil and gas in the Netherlands – is there a future? Neth. J. Geosci. 89-2, 119–135.

Hilger, J., 2003. Combined utilization of oil shale energy and oil shale minerals within the production of cement and other hydraulic binders. Oil shale 20 (3), 347–355.

Hesselbo, S.P., Gröcke, D.R., Jenkyns, H.C., Bjerrum, C.J., Farrimond, P., Morgans Bell, H.S., Green, O.R., 2000. Massive dissociation of gas hydrate during a Jurassic oceanic anoxic event. Nature 406, 392–395.

Houben, M.E., Desbois, G., Urai, J.L., 2013. Pore morphology and distribution in the shaly facies of Opalinus Clay (Mont Terri, Switzerland): insights from representative 2D BIB-SEM investigations on mm to nm scale. Appl. Clay Sci. 71, 82–97.

Houben, M.E., Desbois, G., Urai, J.L., 2014. A comparative study of representative 2D microstructures in Shale and Sandy facies of Opalinus Clay (Mont Terri, Switzerland) inferred from BIB-SEM and MIP methods. Mar. Pet. Geol. 49, 143–161.

Houben, M.E., Barnhoorn, A., Lie-A-Fat, J., Ravestein, T., Peach, C., Drury, M., 2016. Microstructural characteristics of the Whitby Mudstone Formation (UK). Mar. Pet. Geol. http://dx.doi.org/10.1016/j.mapetgeo.2015.11.011.

Holt, R., Fjær, E., Stenebråten, J.F., Nes, O.-M., 2015. Brittleness of shales: Relevance to borehole collapse and hydraulic fracturing. J. Pet. Sci. Eng. 131, 200–209.

Imber, J., Armstrong, H., Clancy, S., Daniels, S., Herringshaw, L., McCaffrey, K., Rodrigues, J., Trabucho-Alexandres, J., Warren, C., 2014. Natural fractures in a United Kingdom shale reservoir analog, Cleveland Basin, northeast England. AAPG Bull. 98 (11), 2411–2437.

Jackson, M.L., Sayin, M., Clayton, R.N., 1976. Hexafluorosilicic acid reagent modification for quartz isolation, soil science society. Am. J. 40, 958–960.

Jarvie, D.N., Hill, R.J., Ruble, T.E., Pollastro, R.M., 2007. Unconventional shale-gas systems: the Mississippian Barnett Shale of north-central Texas as one model for thermogenic shale-gas assessment. Am. Assoc. Pet. Geol. Bull. 91, 475–499.

Kameda, A., Dvorkin, J., Keehm, Y., Nur, A., Bosl, W., 2006. Permeaiblity-porosity transforms from small sandstone fragments. Geophysics 71 (1), N11–N19.

Kanitpanyacharoen, W., Kets, F.B., Wenk, H.-R., Wirth, R., 2012. Mineral preferred orientation and microsturcture in the Posidonia Shale in relation to different degrees of thermal maturity. Clay Clay Miner. 60, 315–329.

Kemp, D.B., Coe, A.L., Cohen, A.S., Schwark, L., 2005. Astronomical pacing of methane release in the Early Jurassic period. Nature 437, 396–399.

Klaver, J., Desbois, G., Urai, J.L., Littke, R., 2012. BIB-SEM study of the pore space morphology in early mature Posidonia Shale from the Hils area, Germany. Int. J. Coal Geol. 103, 12–25.

Klaver, J., Desbois, G., Urai, J.L., Littke, R., 2015a. BIB-SEM characterization of pore space morphology and distribution in postmature to overmature samples from the Haynesville and Bossier shales. Mar. Pet. Geol. 59, 451–466.

Klaver, J., Hemes, S., Houben, M., Desbois, G., Radi, Z., Urai, J.L., 2015b. The connectivity of pore space in mudstones: insights from high-pressure Wood's metal injection, BIB-SEM imaging, and mercury intrusion porosimetry. Geofluids 15 (4), 577–591.

Klaver, J., Desbois, G., Littke, R., Urai, J.L., 2016. BIB-SEM pore characterization of mature and post mature Posidonia Shale samples from the Hils area, Germany. Int. J. Coal Geol. 158, 78–89.

Littke, R., Baker, D.R., Leythaeuser, D., 1988. Microscopic and sedimentologic evidence for the generation and migration of hydrocarbons in Toarcian source rocks of different maturities. Org. Geochem. 13, 549–559.

Littke, R., Baker, D.R., Leythaeuser, D., Rullkötter, J., 1991. Keys to the depositional history of the Posidonia Shale (Toarcian) in the Hils Syncline, northern Germany from In: Tyson, R.V., Pearson, T.H. (Eds.), Modern and Ancient Continental Shelf Anoxia, Geological Society Special publication. Vol. 58, pp. 331–333.

Loucks, R.G., Reed, R.M., Ruppel, S.C., Hammes, U., 2012. Spectrum of pore types and networks in mudrocks and a descriptive classification for matrix-related mudrock pores. AAPG Bull. 96 (6), 1071–1098.

Mathia, E., Bowen, L., Thomas, K.M., Aplin, A.C., 2016. Evolution of porosity and pore types in organic-rich, calcareous, lower Toarcian Posidonia Shale. Mar. Pet. Geol. 75, 117–139.

Moore, D.M., Reynolds, R.C., 1997. X-ray Diffraction and the Identification and Analysis of Clay Minerals. second ed. Oxford university press.
Perez Altamar, R., Marfurt, K., 2015. Mineralogy-based brittleness prediction from surface seismic data: application to the Barnett Shale. Interpretation 2 (4), T255–T271.
Power, M., Burns, S., 2013. The Comparison of QEMSCAN and XRD Analysis in the Mineralogical Characterisation of Unconventional Reservoirs: The Benefits of an Integrated Approach, Geoconvention 2013. Integration, Canada's Energy Geoscientists, CSPG Conferences.
Power, M., Bonijoly, D., Hofmann, A., Rigollet, C., Simpson, M., 2014. The role of mineralogy (QEMSCAN) in the facies heterogeneity characterization or organic rich shale. 76th EAGE Conference and Exhibition 2014. The Netherlands, Amsterdam.
Raiswell, R., Bottrell, S.H., Al-Biatty, H.J., Tan, M.M.D., 1993. The influence of bottom water oxygenation and reactive iron content on sulphur incorporation into bitumens from Jurassic marine shales. Am. J. Sci. 293, 569–596.
Rexer, T.F., Mathia, E.J., Aplin, A.C., Thomas, K.M., 2014. High-pressure methane adsorption and characterization of pores in Posidonia Shales and isolated kerogens. Energy Fuel 28, 2886–2901.
Rietveld, H.M., 1967. Line profiles of neutron powder-diffraction peaks for structure refinement. Acta Cryst 22, 151.
Röhl, H.-J., Schmid-Röhl, A., Oschmann, W., Frimmel, A., Schwark, L., 2001. The Posidonia Shale (Lower Toarcian) of SW-Germany: an oxygen-depleted ecosystem controlled by sea level and palaeoclimate. Palaeogeogr. Palaeoclimatol. Palaeoecol. 165, 27–52.
Rullköter, J., Leythaeuser, D., Horsfield, B., Littke, R., Mann, U., Müller, P.J., Radke, M., Schaefer, R.G., Schenk, H.-J., Schwochau, K., Witte, E.G., Welte, D.H., 1988. Organic matter maturation under the influence of a deep intrusive source: a natural experiment for quantitation of hydrocarbon generation and expulsion from a petroleum source rock. Adv. Org. Geochem. 13, 847–856.
Rybacki, E., Meier, T., Dresen, G., 2016. What controls the mechanical properties of shale rocks? – part II: brittleness. J. Pet. Sci. Eng. 144, 39–58.
Saelen, G., Tyson, R.V., Telnaes, N., Talbot, M.R., 2000. Contrasting watermass conditions during deposition of the Whitby Mudstone (Lower Jurassic) and Kimmeridge Clay (Upper Jurassic) formations, UK. Palaeogeogr. Palaeoclimatol. Palaeoecol. 163, 163–196.
Scarlett, N.V.Y., Madsen, I.C., 2006. Quantification of phases with partial or no known crystal structure. Powder Diffract. 21 (4), 278–284.
Song, J., Littke, R., Maquil, R., Weniger, P., 2014. Organic facie variability in the Posidonia Black Shale from Luxembourg: implications for thermal maturation and depositional environment. Palaeogeogr. Palaeoclimatol. Palaeoecol. 410, 316–336.
Song, J., Littke, R., Weniger, P., Ostertag-Henning, C., Nelskamp, S., 2015. Shale oil potential and thermal maturity of the lower Toarcian Posidonia Shale in NW Europe. Int. J. Coal Geol. 150-151, 127–153.
Środoń, J., Drits, V.A., McCarty, D.K., Hsieh, J.C.C., Eberl, D.D., 2001. Quantitative X-ray diffraction analysis of clay-bearing rocks from random preparations. Clay Clay Miner. 49 (6), 514–528.
Ter Heege, J., Zijp, M., Nelskamp, S., Douma, L., Verreussel, R., ten Veen, J., de Bruin, G., Peters, R., 2015. Sweet sport identification in underexplored shales using multidisciplinary reservoir characterization and key performance indicators: example of the Posidonia Shale Formation in the Netherlands. J. Nat. Gas Sci. Eng. 27, 558–577.
Tissot, B.P., Welte, D.H., 1978. Petroleum Formation and Occurrence. Vol. 451. Springer.
Trabucho-Alexandre, J., Dirkx, R., Veld, H., Klaver, G., de Boer, P.L., 2012. Toarcian black shales in the Dutch Central Graben: record of energetic, variable depositional conditions during an oceanic anoxic event. J. Sediment. Res. 82, 104–120.
Wang, F.P., Gale, J.F.W., 2009. Screening criteria for shale-gas systems, Gulf Coast Assoc. Geol. Soc. Trans. 59, 779–793.
Yang, Y., Sone, H., Hows, A., Zoback, M.D., 2013. Comparison of brittleness indices in organic-rich shale formations. 47th U.S. Rock Mechanics/Geomechanics Symposium, San Francisco, Carlifornia, 23–26 June. American Rock Mechanics Association ARMA-2013-403.
Zhubayev, A., Houben, M.E., Smeulders, D.M.J., Barnhoorn, A., 2016. Ultrasonic velocity and attenuation anisotropy of shales (Whitby, UK). Geophysics 81, D45–D56.
Zijp, M., ten Veen, J., Verreussel, R., ter Heege, J., Ventra, D., Martin, J., 2015. Shale gas formation research: from well logs to outcrop – and back again. First Break 33, 99–106.